Available online at www.sciencedirect.com
SCIENCE DIRECT®
Combustion and Flame 143 (2005) 227–245
Combustion and Flame
www.elsevier.com/locate/combustflame

Premixed flamelet modelling: Factors influencing the turbulent heat release rate source term and the turbulent burning velocity

D. Bradley [a,*], P.H. Gaskell [a], X.J. Gu [b], A. Sedaghat [a,1]

[a] *School of Mechanical Engineering, University of Leeds, Leeds LS2 9JT, UK*
[b] *Department of Computational Science and Engineering, CLRC Daresbury Laboratory, Warrington WA4 4AD, UK*

Received 14 October 2004; received in revised form 20 May 2005; accepted 24 May 2005

Available online 27 July 2005

Abstract

A flamelet approach is adopted in a study of the factors affecting the volumetric heat release source term in turbulent combustion. This term is expressed as the product of an instability enhanced burning rate factor, P_{bi}, and the mean volumetric heat release rate in an unstretched laminar flamelet of the mixture. Included in the expression for P_{bi} are a pdf of the flame stretch rate and a flame stretch factor. Fractal considerations link the turbulent burning velocity normalised by the effective rms turbulent velocity to P_{bi}. Evaluation of this last parameter focuses on problems of (i) the pdfs of the flame stretch rate, (ii) the effects of flame stretch rate on the burning rate, (iii) the effects of any flamelet instability on the burning rate, (iv) flamelet extinctions under positive and negative flame stretch rates, and (v) the effects of the unsteadiness of flame stretch rates. The Markstein number influences both the rate of burning and the possibility of flamelet instabilities developing which, through their ensuing wrinkling, increase the burning rate. The flame stretch factor is extended to embrace potential Darrieus–Landau thermo-diffusive flamelet instabilities. A major limitation is the insufficient understanding of the effects of negative stretch rates that might cause flame extinction. The influences of positive and negative Markstein numbers are considered separately. For the former, a computed theoretical relationship for turbulent burning velocity, normalised by the effective rms velocity, is developed which, although close to that measured experimentally, tends to be somewhat lower at the higher values of the Karlovitz stretch factor. This might be attributed to reduced flame extinction and reduced effective Markstein numbers when the increasingly nonsteady conditions reduce the ability of the flame to respond to changes in flame stretch rates. As the pressure increases, Markstein numbers decrease. For negative Markstein numbers the predicted values of P_{bi} and turbulent burning velocity are significantly increased above the values for positive Markstein numbers. This is confirmed experimentally and these values are close to those predicted theoretically. The increased values are due to the greater stretch rate required for flame extinction, the increased burning rate at positive values of flame stretch rate, and, in some instances, the development of flame instabilities. At lower values of turbulence than those covered by these computations, burning velocities can be enhanced by flame instabilities, as they are with laminar flames, particularly at negative Markstein numbers.
© 2005 The Combustion Institute. Published by Elsevier Inc. All rights reserved.

* Corresponding author.
E-mail address: d.bradley@leeds.ac.uk (D. Bradley).
[1] Current address: Isfahan University of Technology, Isfahan, Iran.

0010-2180/$ – see front matter © 2005 The Combustion Institute. Published by Elsevier Inc. All rights reserved.
doi:10.1016/j.combustflame.2005.05.014

Keywords: Turbulent burning velocity; Instabilities; Source term

1. Introduction

Laminar flames can become unstable and cellular, with an increase in their burning velocity. Several analyses [1–4] also suggest that the burning velocity of turbulent flames might be similarly enhanced. This would appear to be particularly important at high pressures, at which Kobayashi and co-workers [5–7] have reported higher burning velocities than might otherwise have been expected, and attributed these to flame instabilities. Such enhancement would depend on the range of unstable wavelengths of the wrinkled flame and the decrease in Markstein numbers, which often become negative, with increased pressure. Another factor is that mixtures with negative Markstein numbers appear to require higher stretch rates for flame extinction [8].

The paper reports a study of these and other effects. A burning rate factor within the energy source term in the set of CFD equations allows for them and also enables turbulent burning velocities to be found. Comparisons of such velocities with measured values reveal underlying influences on burning rates at high pressure and aid in the formulation of realistic source terms in CFD models.

The formulation of chemical and heat release source terms is central to the mathematical modelling of turbulent combustion [9,10]. The eddy breakup model [11] avoided chemistry and depended only upon turbulent parameters. Since then, detailed chemical reactions have been coupled increasingly with the turbulent flow field. Laminar flamelet modelling has been combined with Reynolds average Navier–Stokes (RANS), Reynolds stress, modelling [12], and also [13] with conditional moment closure (CMC) procedures [14]. The joint probability density function (JPDF) methodology [15] has progressed as have, more recently, large eddy simulations (LES) [16], to which flamelet source terms also are applicable. The variety of approaches has been thoroughly reviewed by Bray et al. [17] and Veynante and Vervisch [18].

Direct numerical simulations (DNS) have shown the flamelet approach to be rather more robust than was originally envisaged by the Klimov–Williams criterion that the flame thickness, δ_ℓ, should be less than the Kolmogorov length scale [19,20]. In the thin reaction zone regime [10] the Kolmogorov scale vortices can be readily accommodated within δ_ℓ, as a consequence of their short lifetime and high curvature. However, the vortices, enlarged by the increased viscosity at the higher temperature, are too large to penetrate the much smaller thickness of the fuel-consuming inner layer. For these reasons, flamelet assumptions are valid up to high values of the Karlovitz stretch factor and this approach is therefore adopted.

The mean volumetric heat release rate, $\bar{q}_t$, can be expressed in terms of that in stretched laminar flamelets, $q_\ell(c,s)$, as a function of the reaction progress variable, c, and the dimensionless flame stretch rate, s, by [21]

$$\bar{q}_t = \int_{s_{q-}}^{s_{q+}} \int_0^1 q_\ell(c,s)\,p(c,s)\,\mathrm{d}c\,\mathrm{d}s, \tag{1}$$

where $p(c,s)$ is a joint pdf of c and s. The stretch rate integral limits, s_{q+} and s_{q-}, are flame extinction stretch rates under positive and negative flame stretch rates. The former and $q_\ell(c,s)$ can be obtained from mathematical models of the specific laminar flames using detailed chemical kinetics.

Direct numerical simulations with detailed chemistry [21,22] suggest that the volumetric heat release rate at a stretch rate, s, can be related to that at zero stretch rate, $q_{\ell 0}(c)$, by [21]

$$q_\ell(c,s) = f(s)q_{\ell 0}(c). \tag{2}$$

Here $f(s)$ is a flame stretch factor, derived from the chemical kinetics, that depends on both s and Markstein numbers of the mixture and $q_{\ell 0}(c)$ is the volumetric heat release rate in an unstretched laminar flame.

If the influences of c and s are statistically independent, $p(c,s)$ may be expressed by the product of the two separate pdfs, $p(c)p(s)$, and

$$\bar{q}_t = P_\mathrm{b} \int_0^1 q_{\ell 0}(c)\,p(c)\,\mathrm{d}c. \tag{3}$$

This conveniently groups flame stretch rate effects together in a burning rate factor, P_b:

$$P_\mathrm{b} = \int_{s_{q-}}^{s_{q+}} f(s)\,p(s)\,\mathrm{d}s. \tag{4}$$

The integral term on the right of Eq. (3) is the mean volumetric heat release rate in unstretched laminar flamelets.

A similar expression to P_b arises in the flame surface density approach [23]. The source term is the mass burning rate, $I_\mathrm{o}\rho_\mathrm{u}u_\ell\Sigma$, where I_o is a factor similar to P_b that expresses the influence of flame stretch [24], ρ_u is the density of the reactants, u_ℓ the unstretched laminar burning velocity, and Σ the flame surface density. The source term, in the form

Nomenclature

A	numerical constant
C_1	numerical constant, see Eq. (B.2a)
C_2	numerical constant, see Eq. (B.2b)
C_s	see Eq. (B.4)
c	reaction progress variable
D	fractal dimension
Da	Damköhler number, $u_\ell l/u'\delta_\ell$
F	fractal factor for turbulent flame wrinkling
f	multiplying factor for theoretical unstable wavenumber, n_s
f	frequency of imposed flame oscillations
$f(s)$	flame stretch factor that expresses effect of flame stretch rate on $q_{\ell 0}(c)$
$f_+(s)$	$f(s)$ for positive values of $\mathrm{Ma_{sr}}$
$f_-(s)$	$f(s)$ for negative values of $\mathrm{Ma_{sr}}$
$f_{+i}(s)$	$f_+(s)$, but in the presence of flame instabilities
$f_{-i}(s)$	$f_-(s)$, but in the presence of flame instabilities
I_o	function that expresses effect of flame stretch rate in flame surface density expression
K	turbulent Karlovitz stretch factor, $(u'/\lambda)(\delta_\ell/u_\ell)$
K_ℓ	laminar Karlovitz stretch factor, $\alpha(\delta_\ell/u_\ell)$
$K_{q\ell+}$	laminar Karlovitz stretch factor for flame extinction by positive stretch, $\alpha_{q+}(\delta_\ell/u_\ell)$
$K_{q\ell-}$	laminar Karlovitz stretch factor for flame extinction by negative stretch, $\alpha_{q-}(\delta_\ell/u_\ell)$
l	integral length scale of turbulence
l_s	cell wavelength at inner cutoff
Le	Lewis number
$\mathrm{Ma_{sr}}$	Markstein number for strain rate, based on reaction zone surface
$(n_l)_\mathrm{cl}$	wavenumber at $\mathrm{Pe_{cl}}$
n_s	largest unstable wavenumber
P_b	burning rate factor
P_bi	P_b, but allowing for flamelet instabilities
$\mathrm{Pe_{cl}}$	critical Peclet number
$p(s)$	pdf of normalised flame stretch rate
$q_\ell(c,s)$	volumetric heat release rate in laminar flamelet
$q_{\ell 0}(c)$	volumetric heat release rate in an unstretched laminar flame
$\bar{q}_t$	mean turbulent volumetric heat release rate
R_l	turbulent Reynolds number based on integral length scale of turbulence
R_λ	turbulent Reynolds number based on Taylor length scale of turbulence
r	spherical flame radius
s	normalised flame stretch rate
S	flame speed factor
s_cl	critical value of s, below which a flamelet becomes unstable
s_{q+}	positive stretch rate for flame extinction
s_{q-}	negative stretch rate for flame extinction
t	time
U	u_t/u'_k
u'	rms turbulent velocity
u'_k	effective rms turbulent velocity acting on flame front
u_ℓ	unstretched laminar burning velocity
u_n	stretched laminar burning velocity based on the rate of disappearance of unburned gas
u_ni	stretched burning velocity after enhancement of u_n due to instabilities
u_nr	stretched laminar burning velocity based on the rate of formation of burned gas
u_nri	stretched burning velocity after enhancement of u_nr due to instabilities
u_t	turbulent burning velocity
α	flame stretch rate, s^{-1}
α_{q+}	positive flame stretch rate for laminar flame extinction, s^{-1}
α_{q-}	negative flame stretch rate for laminar flame extinction, s^{-1}
ϕ	equivalence ratio
δ_ℓ	laminar flame thickness given by ν/u_ℓ
η	Stokes parameter
λ	Taylor length scale of turbulence
$\rho_\mathrm{u}/\rho_\mathrm{b}$	ratio of unburned/burned gas density
ν	kinematic viscosity
τ_η	Kolmogorov time scale

of Eq. (3), has been embedded in the equation set for both premixed [12] and nonpremixed [13] combustion, with a second order Reynolds stress model and second order closure of the reaction progress variable. First and second moments defined the pdfs of appropriately assumed form [12,13,25].

Earlier work [26] assumed $p(s)$ to be simply the pdf of strain rate, $f(s)$ to be unity and s_{q-} to be infinity. The present study employs a recently derived expressions for $p(s)$, with the flame reference surface at the start of the reaction zone, and accounts for the contributions of both strain rate and flame curvature. A linear variation of $f(s)$ with s is assumed, along with laminar flame values for s_{q+} and finite values for s_{q-}. An allowance is introduced for any enhanced burning rate through flamelet wrinkling arising from flamelet instabilities, with a burning rate factor indicated by P_{bi}.

Insofar as these influences affect P_{b}, they also, when combined with fractal wrinkling [27], provide an expression for the turbulent burning velocity, u_t, based on the mass rate of formation of burned gas, given by

$$\frac{u_t}{u'_k} = U = \left(\frac{u_\ell}{u'_k} + F\right) P_{\mathrm{b}}^{0.5} \quad \text{for } u_\ell/u'_k \leqslant 1.0. \tag{5}$$

Here u'_k is the effective rms turbulent velocity in the premixture, that wrinkles the flame front. In the early stages of an explosion this is less than the usual rms turbulent velocity, u' [28]. F is a factor dependent upon the Kolmogorov and turbulent dissipation constants and lies in the range 2.3 ± 0.15.

Evaluation of P_{b} enables values of U to be found from Eq. (5) and compared with those obtained experimentally. This evaluation highlights many of the problems of modelling turbulent combustion and requires a knowledge of:

(i) pdfs of the flame stretch rate, $p(s)$,
(ii) effects of flame stretch rate on the burning rate, $f(s)$,
(iii) how any flamelet instability affects the burning rate,
(iv) flamelet extinction under positive and negative flame stretch rates, s_{q+} and s_{q-}, and
(v) effects due to the unsteadiness of flame stretch rates.

Several of these influences become more important at high pressure. As u'_k/u_ℓ tends to zero, combustion becomes more laminar-like and the present analysis is unsuited to the transitional regime, $u'_k/u_\ell \leqslant 1$. The procedure adopted is, first, to discuss and quantify each of the five influences and then express P_{bi} in terms of the relevant dimensionless groups. Dimensionless turbulent burning velocities are found from P_{bi} and compared with experimental values. This approach leads to a better understanding of both turbulent burning velocities and CFD source terms.

2. The pdf of stretch rates, $p(s)$

The stretch rate, α s^{-1}, is multiplied by the Kolmogorov time, τ_η, to give a dimensionless stretch rate, s. Because $\tau_\eta = \lambda/(u'\sqrt{15})$, where λ is the Taylor microscale,

$$s = \alpha \frac{\lambda}{u'\sqrt{15}}. \tag{6}$$

This scale is related to the integral length scale of turbulence, l, by $\lambda/l = A/R_\lambda$, where A is a numerical constant, taken to be 16. This gives $\lambda/l = (A/R_l)^{1/2}$ and

$$\tau_\eta = 4(l/u')(15R_l)^{-1/2}. \tag{7}$$

The Karlovitz stretch factor K, $(u'/\lambda)(\delta_\ell/u_\ell)$, expresses a ratio of chemical to turbulent lifetimes. More precisely, u'/λ is the rms strain rate on a randomly orientated surface [29]. From the definitions of τ_η and K,

$$\tau_\eta = (\delta_\ell/u_\ell)\big/\left(K\sqrt{15}\right) \tag{8}$$

and

$$s = \alpha(\delta_\ell/u_\ell)\big/\left(K\sqrt{15}\right). \tag{9}$$

With $\delta_\ell = \nu/u_\ell$, where ν is the kinematic viscosity, from Eqs. (7) and (8)

$$K = 0.25(u'/u_\ell)^2 R_l^{-0.5}. \tag{10}$$

In [30] $p(s)$ is computed in terms of K, R_l, and $\mathrm{Ma_{sr}}$, the Markstein number for strain rate, and values are presented graphically. An analytical algebraic expression for $p(s)$, obtained from the integration of Eq. (30a) in [30], is presented in Appendix A. At moderate to high values of K and turbulent Reynolds number, R_l, $p(s)$ is indeed fairly close to the near-Gaussian form for strain rate derived in [29]. There is, however, an increased spread in $p(s)$ at low values of both of these parameters. Low values of $\mathrm{Ma_{sr}}$ also have an important effect.

3. Evaluation of $f(s)$

Numerical simulations with detailed chemical kinetics of stable CH_4–air and C_3H_8–air laminar flames over a wide range of equivalence ratios, ϕ, in [21] led to two empirical expressions for $f(s)$, depending on

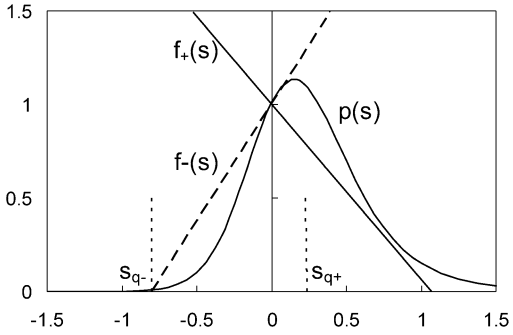

Fig. 1. Typical plots of $f_{+i}(s)$, $f_{-i}(s)$, and $p(s)$.

the sign of $\mathrm{Ma_{sr}}$:

$$f_+(s) = 1 - 0.8(1 - u_{\mathrm{nr}}/u_\ell) \tag{11a}$$

for positive values of both s and $\mathrm{Ma_{sr}}$, and

$$f_-(s) = 1 - 0.8(1 - u_{\mathrm{n}}/u_\ell) \tag{11b}$$

for positive values of s and negative values of $\mathrm{Ma_{sr}}$.

Here u_{nr} is the burning velocity for the rate of formation of burned gas and u_{n} is that for rate of disappearance of unburned gas. The expressions are analogous to those for the relationship among Markstein number, burning velocity, and flame stretch rate. Although only positive stretch rates could be simulated, the appropriate expression for $f(s)$ is applied to laminar flamelets in turbulent combustion throughout the spectrum of s, irrespective of the sign of s. This is justified by both computational [31] and experimental [32] studies which have shown the relationship to hold along the entire wrinkled flamelet surface, irrespective of the sign of s.

From the expressions for u_{nr}/u_ℓ and u_{n}/u_ℓ in terms of s and $\mathrm{Ma_{sr}}$ given in [30] and also as Eqs. (B.2a) and (B.2b) in Appendix B, then

$$f_+(s) = 1 - 0.8s\,\mathrm{Ma_{sr}}\,C_1 K\sqrt{15}$$
$$\text{with } C_1 = 0.925 \tag{12a}$$

and

$$f_-(s) = 1 - 0.8s(\rho_{\mathrm{u}}/\rho_{\mathrm{b}} - 1)\,\mathrm{Ma_{sr}}\,C_2 K\sqrt{15}$$
$$\text{with } C_2 = 1.225. \tag{12b}$$

Typical plots of $f_+(s)$, $f_-(s)$ and $p(s)$ are shown in Fig. 1. The vertical dashed lines indicate values of the flame extinction stretch rates. For a flame stretch rate equal to the rms strain rate, u'/λ, because $\tau_\eta = \lambda/(u'\sqrt{15})$, then in this particular case $s = (15)^{-1/2} = 0.258$. From Eqs. (12a) and (12b) the gradients of the two lines, $\mathrm{d}f_+(s)/\mathrm{d}s$ and $\mathrm{d}f_-(s)/\mathrm{d}s$ are proportional to $-\mathrm{Ma_{sr}}\,K$.

4. Influence of flamelet instability on $f(s)$

The approach adopted is to modify $f(s)$, to take account of the increased flamelet area arising from Darrieus–Landau thermo-diffusive instabilities in flamelets. A sufficiently high stretch rate stabilises a laminar flame, but when it falls below a critical value, s_{cl}, the flame becomes unstable and wrinkles. The method of determining s_{cl} from observations of explosion flames is described in Appendix B.

In the unstable stretch regime $s_{\mathrm{cl}} \geqslant s \geqslant s_{q-}$, the expression for $f_+(s)$ in Eq. (11a) becomes

$$f_{+i}(s) = 1 - 0.8(1 - u_{\mathrm{nri}}/u_\ell)$$
$$\text{for positive values of } \mathrm{Ma_{sr}}, \tag{13a}$$

$$f_{-i}(s) = 1 - 0.8(1 - u_{\mathrm{ni}}/u_\ell)$$
$$\text{for negative values of } \mathrm{Ma_{sr}}. \tag{13b}$$

Here the additional subscript "i" indicates a stretched burning velocity enhanced by the wrinkling from the instabilities. The ratio of the enhanced area to the original flame area quantifies the ratios, $u_{\mathrm{nri}}/u_{\mathrm{nr}}$ and $u_{\mathrm{ni}}/u_{\mathrm{n}}$. The area ratio is found from the inner, l_s, and outer, l, wavelength cutoffs and the fractal dimension, D. Consequently [26],

$$u_{\mathrm{nri}}/u_{\mathrm{nr}} = (l/l_s)^{D-2}$$
$$\text{for positive values of } \mathrm{Ma_{sr}} \tag{14a}$$

and

$$u_{\mathrm{ni}}/u_{\mathrm{n}} = (l/l_s)^{D-2}$$
$$\text{for negative values of } \mathrm{Ma_{sr}}. \tag{14b}$$

Laminar spherical flame instabilities have been analysed in this way [33,34]. For turbulent flames a value of 7/3 has been assigned to D [5,26] and this gave rise to Eq. (5). This value of D has been employed also in large-scale, initially laminar, explosions [35–37] to give the ratio of burning velocities.

The outer cutoff wavelength, l, is assumed to be the integral length scale. When normalised by δ_ℓ, this gives

$$(l/\delta_\ell) = 0.5R_l^{0.75}K^{-0.5}. \tag{15}$$

Instability only occurs when $l/l_s > 1$. Experimental studies of cellular flames in spherical explosions [38] have shown how flame instability at the longer wavelengths creates a cascade of progressively decreasing unstable wavelengths. This terminates when the localised stretch rate at the inner cutoff is sufficiently high for localised thermo-diffusion to stabilise the flame. There would appear to be some universality of structure at the inner cutoff, irrespective of the outer cutoff and this concept is employed to evaluate

l_s/δ_ℓ. Evaluation of l_s/δ_ℓ under different conditions is described in Appendix B. With Eq. (15) this enables l/l_s in Eq. (14) to be found and ultimately a burning rate factor that allows for instabilities, $P_{\rm bi}$.

An instability band of stretch rates is introduced into Eq. (4) for $P_{\rm b}$, to give $P_{\rm bi}$. For positive values of $\mathrm{Ma_{sr}}$ the stable and unstable contributions to $f_{+i}(s)$ are derived in Appendix B and given as Eq. (B.10a). This yields

$$P_{\rm bi} = \int_{s_{q-}}^{s_{q+}} f_+(s)p(s)\,\mathrm{d}s + \int_{s_{q-}}^{s_{\rm cl}} 0.8\big((l/l_s)^{1/3}-1\big) \times \big(1 - s\,\mathrm{Ma_{sr}}\,C_1K\sqrt{15}\big)p(s)\,\mathrm{d}s, \tag{16a}$$

with $f_+(s)$ given by Eq. (12a). A similar approach for negative values of $\mathrm{Ma_{sr}}$ gives Eq. (B.10b) and

$$P_{\rm bi} = \int_{s_{q-}}^{s_{q+}} f_-(s)p(s)\,\mathrm{d}s + \int_{s_{q-}}^{s_{\rm cl}} 0.8\big((l/l_s)^{1/3}-1\big) \times \big(1 - s(\rho_{\rm u}/\rho_{\rm b}-1)\,\mathrm{Ma_{sr}}\,C_2K\sqrt{15}\big)p(s)\,\mathrm{d}s, \tag{16b}$$

with $f_-(s)$ given by Eq. (12b).

The first integrals on the right of Eqs. (16a) and (16b) are $P_{\rm b}$, while the second integrals represent the additional influence of the instabilities. Equations (15) and (B.7) show the ratio (l/l_s), and hence $P_{\rm bi}$ and U, to be enhanced by high R_l, low K, and small values of $\mathrm{Pe_{cl}}$ (and hence $\mathrm{Ma_{sr}}$). This is in line with previous analyses of the Darrieus–Landau instability [1–4]. Instabilities also arise with laminar and transitional flames when $u'_k/u_\ell \leqslant 1$. The analytical approaches are somewhat different for these conditions.

5. Flame extinction stretch rates

Values of positive stretch rates, α_{q+} $\mathrm{s^{-1}}$, for laminar flame extinction have been obtained from both mathematical models of stretched laminar flames and experiments, almost exclusively at atmospheric pressure. From Eq. (9),

$$s_{q+} = \alpha_{q+}(\delta_\ell/u_\ell)\big/\big(K\sqrt{15}\big). \tag{17}$$

A corresponding laminar Karlovitz stretch factor for flame extinction can be defined by

$$K_{q\ell+} = \alpha_{q+}(\delta_\ell/u_\ell) \tag{18}$$

and hence

$$s_{q+} = K_{q\ell+}\big/\big(K\sqrt{15}\big). \tag{19}$$

This last relationship indicates how an increase in K decreases the value of s_{q+} in Fig. 1.

Table 1
Premixed flame characteristics associated with measured positive quench values for C_3H_8–air flames at 100 kPa and 300 K (α_{q+} and u_ℓ from [8], $\mathrm{Ma_{sr}}$ from [21])

ϕ	u_ℓ (m/s)	$\nu\times10^5$ ($\mathrm{m^2/s}$)	$\mathrm{Ma_{sr}}$	Le	α_{q+} ($\mathrm{s^{-1}}$)	$K_{q\ell+}$
0.7	0.234	1.745	6.17	1.823	350	0.112
0.8	0.312	1.738	6.03	1.790	850	0.152
0.9	0.376	1.732	6.12	1.806	1280	0.157
1.0	0.424	1.725	5.91	1.264	1640	0.157
1.1	0.438	1.718	5.26	0.974	1840	0.165
1.2	0.410	1.712	3.60	0.965	1890	0.192
1.3	0.319	1.706	1.29	0.957	1800	0.302
1.4	0.180	1.700	−0.08	0.949	1560	0.819
1.5	0.106	1.693	−0.53	0.941	1175	1.770
1.6	0.083	1.687	−1.07	0.934	740	1.812

Table 2
Premixed flame characteristics associated with measured positive quench values for CH_4–air flames at 100 kPa and 300 K (α_{q+} and u_ℓ from [8], $\mathrm{Ma_{sr}}$ from [22])

ϕ	u_ℓ (m/s)	$\nu\times10^5$ ($\mathrm{m^2/s}$)	$\mathrm{Ma_{sr}}$	Le	α_{q+} ($\mathrm{s^{-1}}$)	$K_{q\ell+}$
0.55	0.089	1.564	1.71	1.0098	140	0.276
0.60	0.128	1.565	1.96	1.0100	300	0.287
0.70	0.210	1.567	2.68	1.0103	770	0.274
0.80	0.285	1.569	3.09	1.0106	1250	0.241
0.84	0.310	1.570	3.36	1.0107	1520	0.248
0.90	0.345	1.571	3.52	1.0109	1650	0.218
1.00	0.378	1.573	3.85	1.0461	1680	0.185
1.10	0.383	1.575	4.14	1.0838	1230	0.132
1.20	0.320	1.577	4.26	1.0842	760	0.117
1.30	0.160	1.576	3.96	1.0846	470	0.289
1.40	0.135	1.577	3.94	1.0849	240	0.208

Tables 1 and 2 present the experimental values of u_ℓ and α_{q+} from Law et al. [8] for a wide range of ϕ for propane–air and methane–air mixtures. From these are derived, using $\delta_\ell = \nu/u_\ell$, the values of $K_{q\ell+}$ in the final column. These measurements were with symmetric ("unburned to unburned"), steady-state, counterflow flames, under atmospheric conditions. Computed values of $\mathrm{Ma_{sr}}$ from [21] and [22], respectively, also are listed. There is significantly less spread in $K_{q\ell+}$ for mixtures with positive $\mathrm{Ma_{sr}}$ than in α_{q+} and this use of the flame extinction Karlovitz stretch factor gives a useful degree of generalisation [39]. The asymmetric ("burned to unburned") counterflow configuration is perhaps more representative of turbulent flamelet conditions and exhibits a less sharply defined stretch rate at flame extinction. Allowance for this effect (see Eq. (43) in [39]) is made by the last term in

$$s_{q+} = \frac{\alpha_{q+}}{K\sqrt{15}}\left(\frac{\delta_\ell}{u_\ell}\right) - \frac{0.014K}{K\sqrt{15}}$$

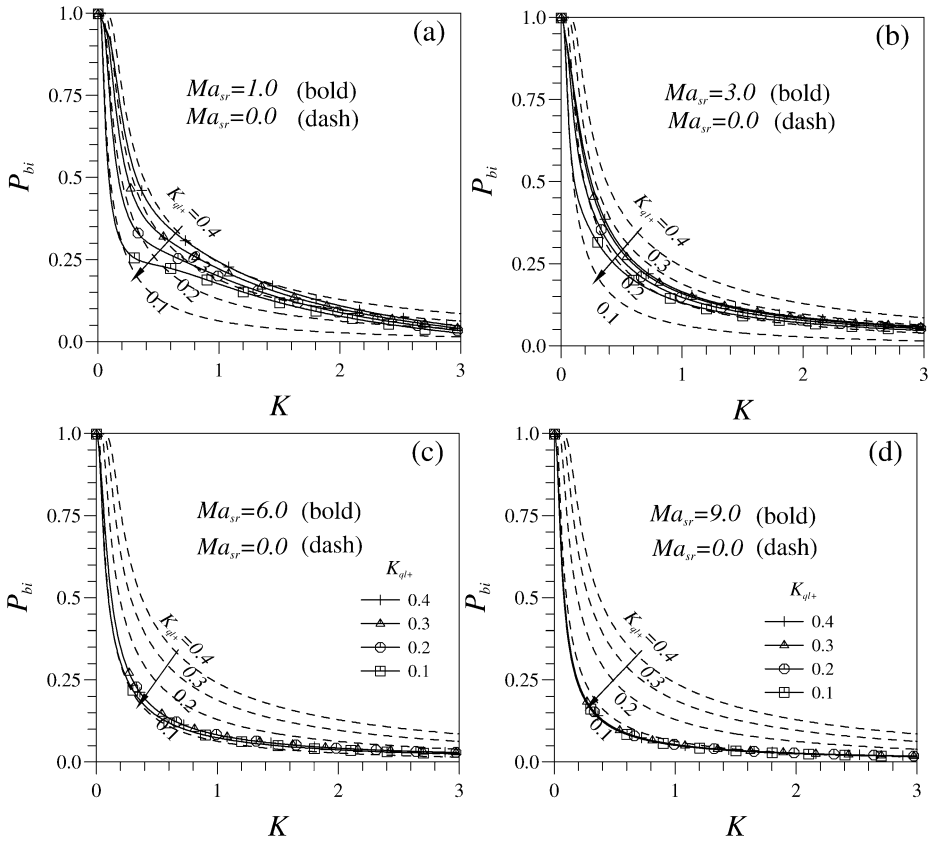

Fig. 2. P_{bi} versus K for four different positive values of $\mathrm{Ma_{sr}}$ and $K_{q\ell+}$ at $R_l = 1000$. Solid curves: s_{q-} based on Eq. (22). Dashed curves: $\mathrm{Ma_{sr}} = 0$ and $f_+(s) = 1.0$, $s_{q-} = -2.5 s_{q+}$.

$$= \frac{K_{q\ell+}}{K\sqrt{15}} - \frac{0.014}{\sqrt{15}}. \tag{20}$$

However, because there can be no significant contribution to combustion from "negative burning velocities" [30] for positive values of $\mathrm{Ma_{sr}}$, flame extinction must effectively occur if $u_{\mathrm{nr}} \leqslant 0$ in Eq. (B.2a). Hence s_{q+} was taken as the smaller of the two values, so that

$$s_{q+} = \min\left(\left(\frac{K_{q\ell+}}{K\sqrt{15}} - \frac{0.014}{\sqrt{15}}\right), \left(\frac{1}{\mathrm{Ma_{sr}}\, 0.925 K\sqrt{15}},\ \mathrm{Ma_{sr}} > 0\right)\right). \tag{21}$$

There are few data related to flame extinction by negative stretch rates, α_{q-}. There was no indication of flame extinction in either computations of spherical implosions over a range of negative stretch rates [22] or experimental measurements of burning velocity with negative stretch rates up to almost 6000 s^{-1} on a slot burner [40]. Nor is there any indication of flame extinction in the negatively stretched, inwardly propagating, flame with a positive value of $\mathrm{Ma_{sr}}$ in [41]. On the other hand, extinction by negative stretch at cusps of large curvature is observed in cellular flames [27,38].

In this uncertain situation, the procedure adopted was to define s_{q-} by proscribing negative burning velocities and applying the condition for flame extinction $u_{\mathrm{n}} \leqslant 0$ in Eq. (B.2b). Hence,

$$s_{q-} = \left[(\rho_{\mathrm{u}}/\rho_{\mathrm{b}} - 1)\,\mathrm{Ma_{sr}}\, C_2 K\sqrt{15}\right]^{-1}, \tag{22}$$

with the values of C_2 given in Eq. (B.2b). For the special condition of $\mathrm{Ma_{sr}} = 0$, which would unrealistically imply s_{q-} to be infinite, s_{q-} was taken to be $-2.5 s_{q+}$.

6. Evaluation of P_{bi} and U for positive values of $\mathrm{Ma_{sr}}$

The applications of Eqs. (16a) and (16b) are discussed separately. The former, for positive values $\mathrm{Ma_{sr}}$, is considered first, for $R_l = 1000$. Shown by the full line curves in Figs. 2a–2d are computed values of P_{bi} for $\mathrm{Ma_{sr}} = 0$, 1, 3, 6, and 9, respectively, plotted against K, for values of $K_{q\ell+} = 0.1$, 0.2, 0.3,

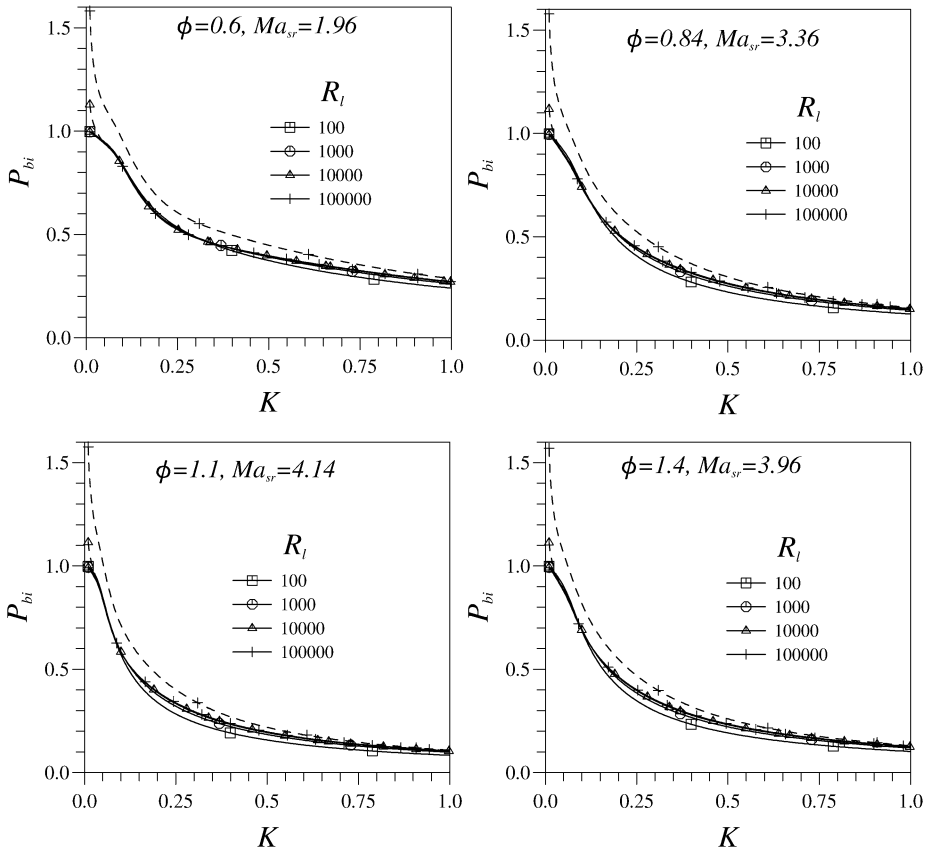

Fig. 3. P_{bi} versus K for four CH_4–air mixtures and four values of R_l. Solid curves: no instability. Dashed curves: with instability.

and 0.4. Tables 1 and 2 suggest that $K_{q\ell+}$ is unlikely to exceed 0.3 for positive values of $\mathrm{Ma_{sr}}$. There is no influence of any flamelet instability in these regimes, as l is always less than l_s. With no flamelet quenching $K_{q\ell+}=\infty$ and $s_{q+}=\infty$. If, in addition, there is no other influence of flame stretch rate, $\mathrm{Ma_{sr}}=0$, it follows from Eq. (12a) that $f_+(s)=1.0$. When these two sets of conditions are combined, then $P_{\mathrm{b}}=1.0$ for all values of K.

The dashed curves are for flamelet extinction alone at the four different values of $K_{q\ell+}$, with no other influence of flame stretch: namely, $\mathrm{Ma_{sr}}=0$ and $f_+(s)=1.0$. The lower the value of K_{ql+}/K, and hence s_{q+} (see Eq. (20)), the lower the value of P_{b}. This follows from the narrowing of the limits of integration of Eq. (16a). Reference to Fig. 2a and comparisons with the full line curves show that the principal reason for the decrease in P_{bi} with K is flame quenching, rather than changes in $f_+(s)$. At higher values of $\mathrm{Ma_{sr}}$ the decrease in $f_+(s)$ with increasing values of s becomes more important. Because, as shown in Fig. 1, $p(s)$ is skewed to positive values of s where $f_+(s)$ is smaller, the full line curves fall increasingly below the dashed curves as $\mathrm{Ma_{sr}}$ increases. Furthermore, the values of s_{q+} are determined by the condition of $u_{\mathrm{nr}}=0$ rather than by $K_{q\ell+}$ at the higher values of $\mathrm{Ma_{sr}}$, see Eq. (21). There is a tendency for P_{bi} to be independent of $K_{q\ell+}$ with increasing $\mathrm{Ma_{sr}}$, as can be seen in Figs. 2c and 2d. Ultimately P_{bi} becomes independent of $K_{q\ell+}$.

Shown in Fig. 3 are plots of P_{bi}, evaluated from Eq. (16a), against K for four methane–air mixtures, $\phi=0.6$, 0.84, 1.1, and 1.4, with the appropriate values of s_{q+}, $\mathrm{Ma_{sr}}$, and $\rho_{\mathrm{u}}/\rho_{\mathrm{b}}$. Similar plots for three propane–air mixtures, $\phi=0.7$, 1.0, and 1.2, are shown in Fig. 4. Property values are given in Tables 1 and 2. Because $p(s)$ also depends upon R_l, this is specified with values of 100, 1000, 10,000, 100,000. In both sets of figures, only at the last two values of R_l are instability enhancements significant and P_{bi} becomes greater than unity. For these values of R_l two curves are shown: the upper, broken curves are those in which allowance is made for instability. Otherwise the value of R_l has little effect.

Corresponding values of U, found with P_{bi} substituted in Eq. (5) and with $F=2.3$, also are plotted in Fig. 5 for the four CH_4–air mixtures, and in Fig. 6 for the three C_3H_8–air mixtures. Here it was assumed

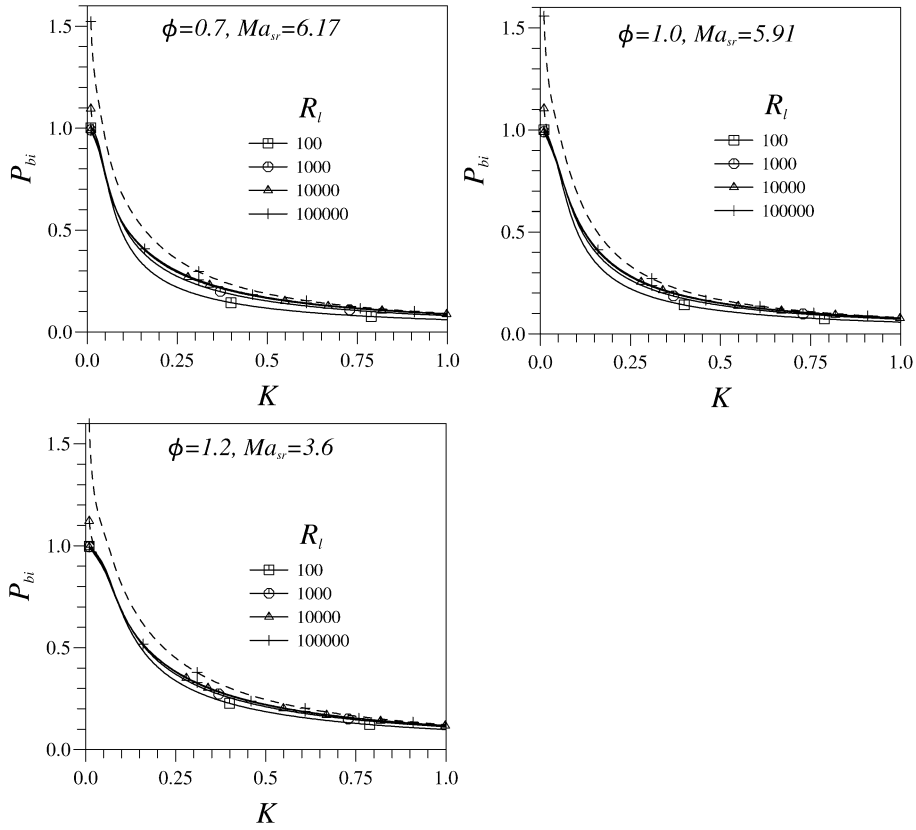

Fig. 4. P_{bi} versus K for three C_3H_8–air mixtures with $\mathrm{Ma_{sr}} > 0$ and four values of R_l. Solid curves: no instability. Dashed curves: with instability.

$u'_k = u'$ and u'/u_ℓ was found from Eq. (10). Also shown by the full line curve is the relationship for U given in [39], in the form presented in [27], with K defined by Eq. (10) and the value of Lewis number, Le, appropriate to the mixture:

$$U = 1.01(K\,\mathrm{Le})^{-0.3} \quad \text{for } 0.02 \leqslant K\,\mathrm{Le} \leqslant 1.0. \tag{23}$$

This equation represents an extensive correlation of 1650 measurements of u_t, principally close to atmospheric pressure and with positive values of $\mathrm{Ma_{sr}}$ [39]. This expression is compared with other expressions for U in [10] and [27]. In the former, U is expressed as a function of the Damköhler number, Da.

Figs. 7–9 show values of U computed from Eqs. (16a) and (5) for all those mixtures in Tables 1 and 2 with positive values of $\mathrm{Ma_{sr}}$. They are plotted against K, K Le, and $K\,\mathrm{Ma_{sr}}$, respectively, for $R_l = 1000$ and $0.02 \leqslant K \leqslant 3.0$. The figures demonstrate progressively improving correlations that correspond with improving allowances for thermo-diffusive effects. This is not surprising, as one of the thrusts of the paper is the importance of the influence of Markstein number. The quite good correlation with $K\,\mathrm{Ma_{sr}}$ is possibly enhanced by what may be perceived from Tables 1 and 2 as a degree of correlation between $\mathrm{Ma_{sr}}$ and $K_{q\ell+}$. Earlier experimental studies of turbulent flame quenching had shown the importance of thermo-diffusive effects and K Le was used to define turbulent quenching limits in [42]. The experimental values are close to those subsequently obtained from direct simulations of flame–vortex interactions that yielded the quenched fraction of the flame surface [43]. Each equivalence ratio in Tables 1 and 2, for which $\mathrm{Ma_{sr}}$ is positive, is represented by a symbol.

The best-fit relationships for each of these curves are shown in Figs. 7–9, in the form $U = Bx^b$, where B and b are constants, and x is, in turn, K, K Le, and $K\,\mathrm{Ma_{sr}}$. Linear regression gave best-fit relationships:

$$U = 0.81K^{-0.42} \quad \text{for } 0.05 \leqslant K \leqslant 3, \tag{24}$$

$$U = 0.86(K\,\mathrm{Le})^{-0.43} \quad \text{for } 0.05 \leqslant K\,\mathrm{Le} \leqslant 5.5, \tag{25}$$

$$U = 1.41(K\,\mathrm{Ma_{sr}})^{-0.43} \quad \text{for } 0.05 \leqslant K\,\mathrm{Ma_{sr}} \leqslant 19. \tag{26}$$

The values of standard deviations from the respective expressions in K, K Le, and $K\,\mathrm{Ma_{sr}}$ are 0.228, 0.182,

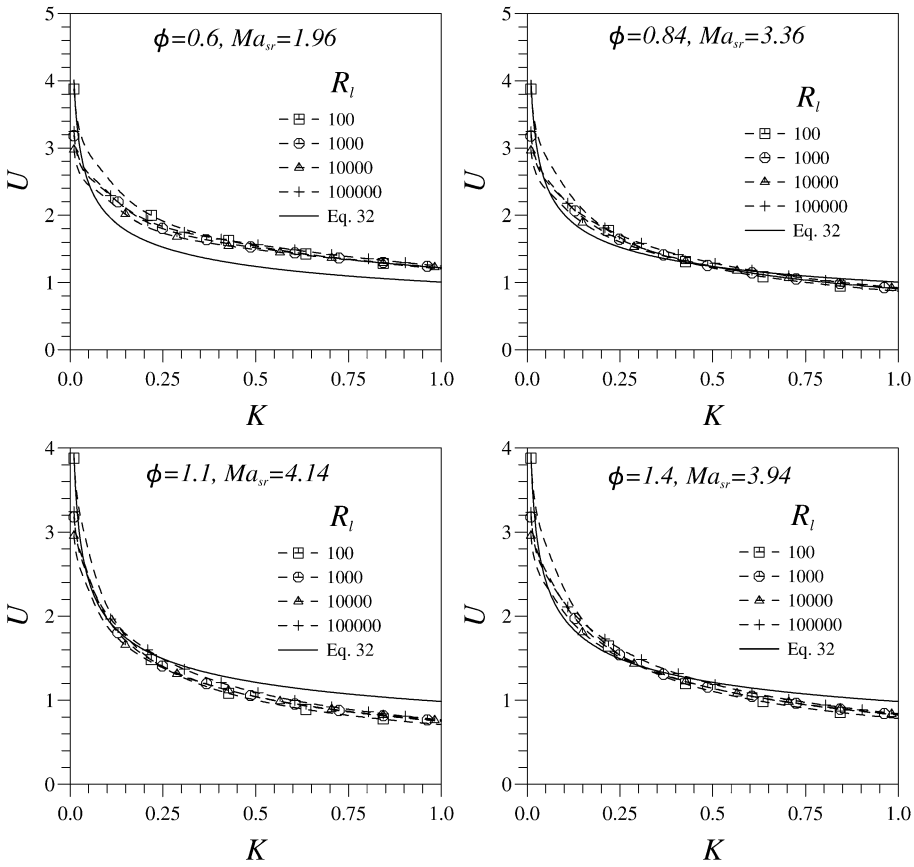

Fig. 5. U versus K for four CH_4–air mixtures and four values of R_l, with instability. Solid curve is Eq. (23).

and 0.095. Also shown in Fig. 9 for comparison are the values of U obtained from Eq. (23), with the value of Le corresponding to CH_4–air at $\phi = 1.1$.

7. Effects of unsteady flame stretch rates

Most values of Markstein numbers and almost all those of α_{q+} have been found with steady-state stretched flames. However, stretch rates are unsteady in both laminar explosions and turbulent flames and questions arise as to the wider applicability of steady-state parameters. In their numerical study of strained (there was no curvature) laminar counterflow diffusion flames Egolfopoulos and Campbell [44] imposed oscillatory changes to the flow and strain rate. The response of the flame was quasi-steady at low frequencies, but amplitudes of the induced oscillations were reduced and phase-shifted at higher frequencies. They defined a Stokes parameter, η,

$$\eta = (\pi \mathrm{f}/\alpha)^{1/2}, \tag{27}$$

in which f is the frequency of the imposed oscillations. In Eq. (27) the original strain rate has been replaced by the flame stretch rate, α. Amplitudes of the induced oscillations in temperature rapidly decreased as η was increased above unity. At still higher values of η the flame no longer responded to the oscillations of the external field.

The effective value of η in laminar spherical explosions at constant pressure is close to unity and computed values of burning velocity based on Markstein lengths obtained from propagating spherical flames are in fair agreement with those measured in steady-state symmetric counterflow flames [22]. As a rough guide as to whether flamelets might locally extinguish in turbulent flames, f in Eq. (27) is taken to be u'/λ, which is the reciprocal time associated with a coherent eddy of the Taylor length scale. The stretch rate is taken to be that for steady-state flame extinction, α_{q+}. With Eq. (18) and the definition of K, Eq. (27) gives

$$\eta = (\pi K/K_{q\ell+})^{1/2}. \tag{28}$$

From Eqs. (19) and (28),

$$\eta = (0.258\pi/s_{q+})^{1/2}. \tag{29}$$

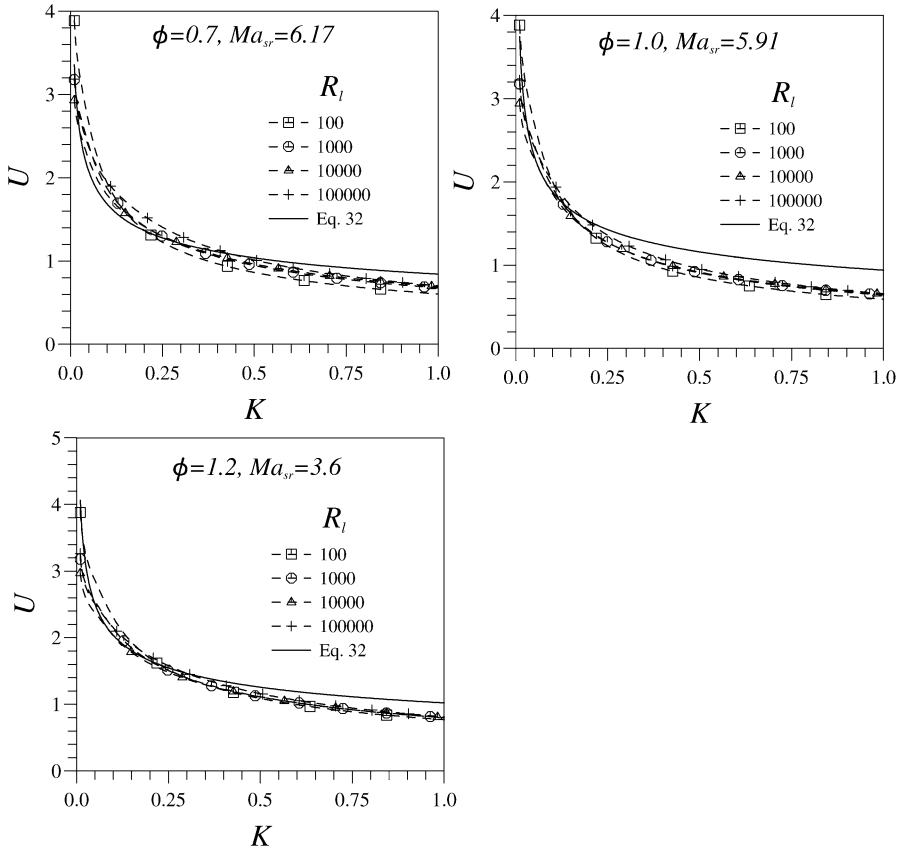

Fig. 6. U versus K for three C_3H_8–air mixtures and four values of R_l, with instability. Solid curve is Eq. (23).

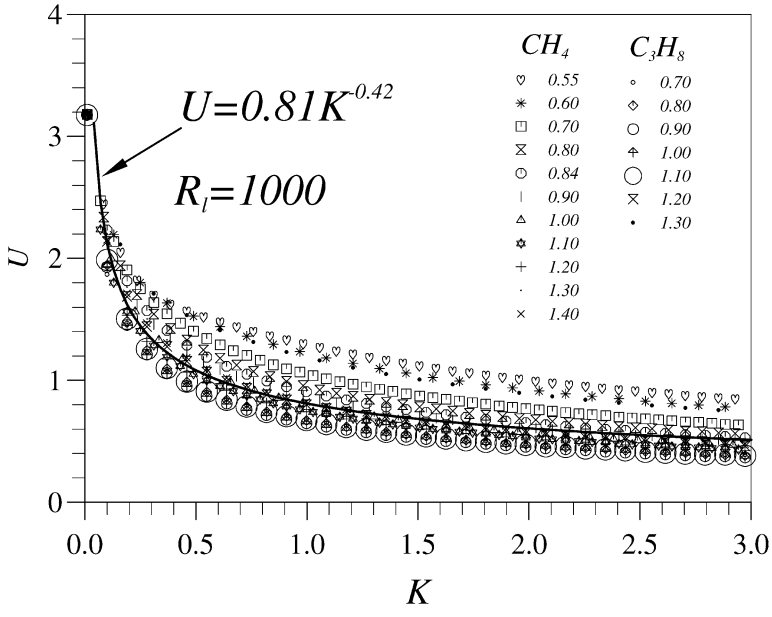

Fig. 7. Correlation of U with K. $R_l = 1000$ for all mixtures with $Ma_{sr} > 0$ listed in Tables 1 and 2.

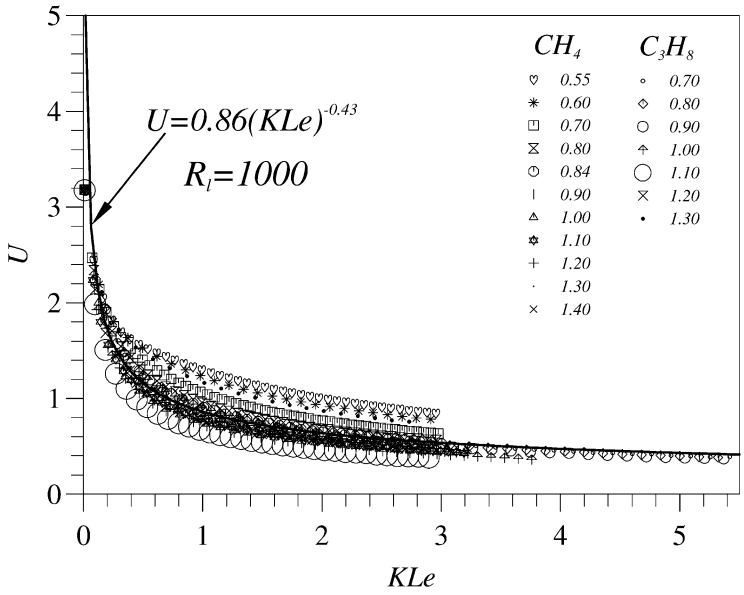

Fig. 8. Correlation of U with K Le. $R_l = 1000$ for all mixtures with $\mathrm{Ma_{sr}} > 0$ listed in Tables 1 and 2.

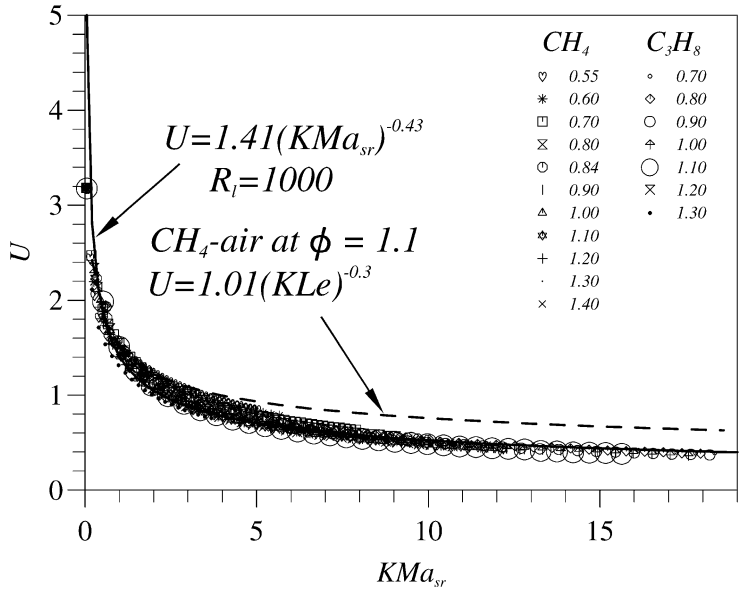

Fig. 9. Correlation of U with K $\mathrm{Ma_{sr}}$. $R_{l=}1000$ for all mixtures with $\mathrm{Ma_{sr}} > 0$ listed in Tables 1 and 2.

For the response of the flame to be quasi-steady with $\eta \leqslant 1$, then, $K \leqslant 0.32 K_{q\ell+}$, from Eq. (28), or $s_{q+} \geqslant 0.81$, from Eq. (29).

The first condition is only fulfilled for the positive values of $\mathrm{Ma_{sr}}$ in Tables 1 and 2 at small values of K, less than about 0.1. This suggests that many turbulent flames might not be extinguishing at stretch rates greater than their steady-state flame extinction stretch rates. The optical diagnostic studies of Donbar et al. [45] of high Reynolds number, nonpremixed, jet flames confirm that flamelets do not locally extinguish at high turbulent frequencies, during brief excursions of stretch rate to well in excess of α_{q+}.

The resulting apparent increase in the value of α_{q+} implies corresponding apparent increases in $K_{q\ell+}$ and s_{q+}. The consequent increase in the in-

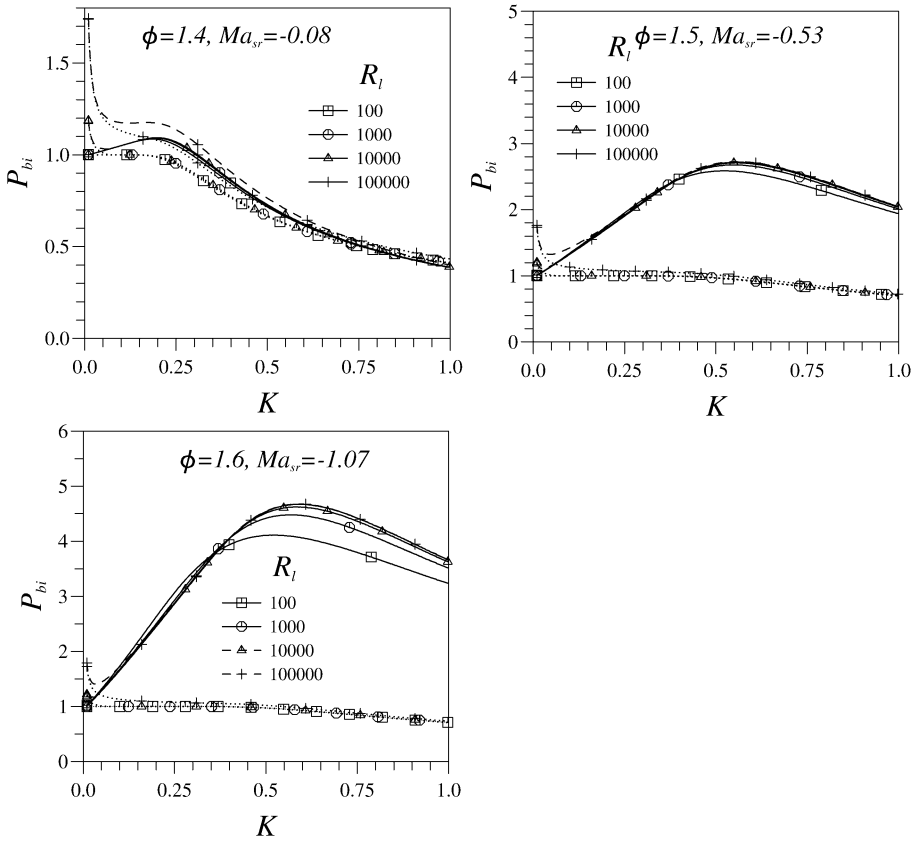

Fig. 10. P_{bi} versus K for three C_3H_8–air mixtures, with $\mathrm{Ma_{sr}} < 0$ and four values of R_l indicated by symbols. Solid curves: no instability. Upper dashed curves: with instability. Lower dotted curves: $\mathrm{Ma_{sr}} = 0$, $f_-(s) = 1.0$.

tegration limits of Eq. (16a) would increase P_{bi} and U. From Eq. (28) this effect should increase roughly as $\sqrt{K}$. Indeed, the experimental correlation of Eq. (23) does give progressively higher values of U than those computed as K increases, as can be seen from Figs. 5, 6, and 9. The effect of nonsteady stretch rates is not confined to $K_{q\ell+}$. The apparent values of $\mathrm{Ma_{sr}}$ also can be changed. Chen and Im [31] observed an apparent decrease in the Markstein number in their numerical simulations as the ratio of chemical to turbulent time increased. The present study cannot separate the effects of unsteadiness on $\mathrm{Ma_{sr}}$ and $K_{q\ell+}$, but apparent values of $\mathrm{Ma_{sr}}$ and $K_{q\ell+}$ can be selected such that the computed values of U are the same as those of experiment. For example, for the C_3H_8–air mixture, $\phi = 1.2$, with $\mathrm{Ma_{sr}} = 3.6$ and $K_{q\ell+} = 0.192$ in Table 1, the computed value of U at $K = 1.0$ is equal to that given by Eq. (23), with $\mathrm{Ma_{sr}} = 2.0$ and $K_{q\ell+} = 0.3$. Changing $K_{q\ell+}$ alone cannot give this equality, since the value of $p(s)$ at s_{q+} is too small. The reduction of $\mathrm{Ma_{sr}}$ and increase of $K_{q\ell+}$ are both necessary to increase the value of U.

8. Evaluation of P_{bi} and U for negative values of $\mathrm{Ma_{sr}}$

Shown by the upper broken line curves in Fig. 10 are values of P_{bi}, evaluated from Eq. (16b) for four different values of R_l and the values of s_{q+}, $\mathrm{Ma_{sr}}$, and $\rho_{\mathrm{u}}/\rho_{\mathrm{b}}$ corresponding to the three propane–air mixtures with negative values of $\mathrm{Ma_{sr}}$ in Table 1. Values of P_{bi} are plotted against K for $\mathrm{Ma_{sr}} = -0.08$, -0.53, and -1.07 and the corresponding values of $K_{q\ell+} = 0.819$, 1.770, and 1.812, respectively. Values of $\mathrm{Pe_{cl}}$ are obtained from Eq. (B.5) and of s_{cl} from Eq. (B.3). The lower dotted curves are for flamelet quenching at the respective value of $K_{q\ell+}$ but with $\mathrm{Ma_{sr}} = 0$, so that from Eq. (12b), $f_-(s) = 1.0$: there are no flame stretch rate effects other than extinction. Comparisons of these lower values of P_{bi} for the dotted curves in Fig. 10 with the dashed curves in Fig. 2 for positive values of $\mathrm{Ma_{sr}}$ show the former to generate significantly higher values of P_{bi}, which decline only slightly with increasing K. This is a consequence of the markedly higher values of $K_{q\ell+}$ for the negative values of $\mathrm{Ma_{sr}}$.

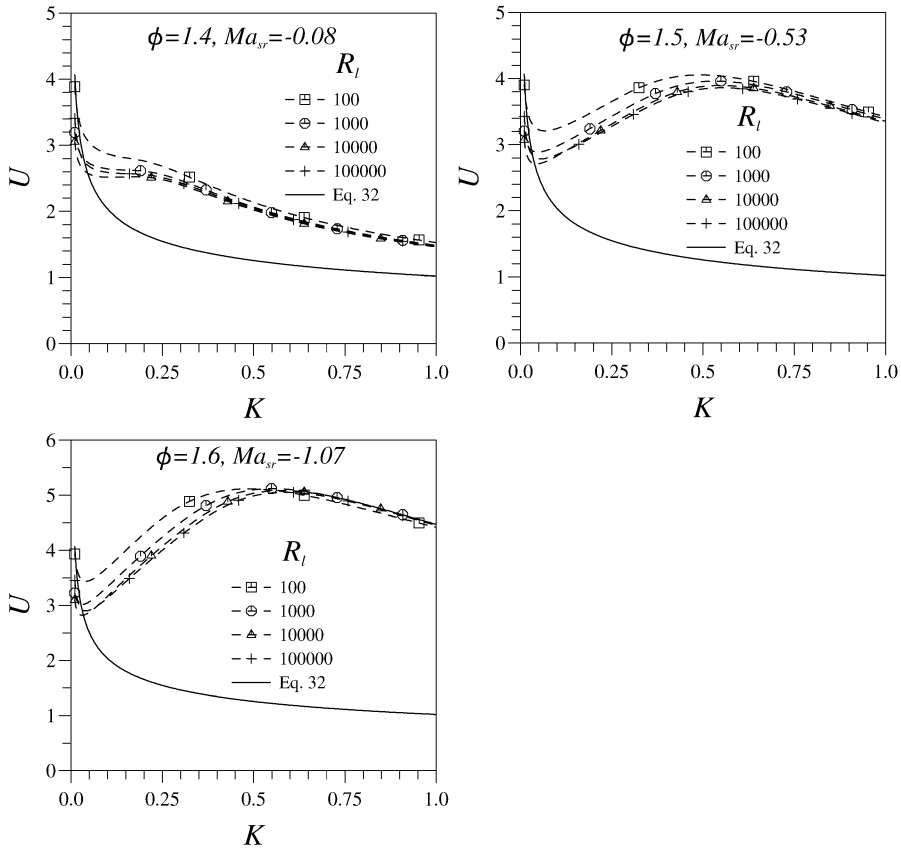

Fig. 11. U versus K for three C_3H_8–air mixtures, with $Ma_{sr} < 0$ and four values of R_l with instability. Solid curve is Eq. (23).

Equation (B.10b) and Fig. 1 show that $f_{-i}(s)$ increases with s for negative values of Ma_{sr}. Because $p(s)$ is skewed to positive values of s for $R_l \geqslant 100$ [30] where $f_{-i}(s)$ is larger, the values of P_{bi} become larger than those of the lower dotted curves and are shown by the upper broken line curves in Fig. 10. For these topmost curves, which include instability effects, the maximum values of P_{bi} become even higher as Ma_{sr} becomes more negative. The extent to which the increase is due to instabilities can be gauged from the solid line curves in Fig. 10. These give values of P_b when no allowance is made for instability effects. Such effects are only significant at the highest values of R_l and at low values of K. For positive values of Ma_{sr} and no instability effects $P_b \leqslant 1.0$. With these effects the burning rate factor exceeds unity.

The corresponding values of U, found by substituting values of P_{bi} from Fig. 10 into Eq. (5) with $F = 2.3$ are plotted in Fig. 11. The high values of P_{bi} give rise to exceptionally high values of U, significantly greater than those given by Eq. (23), which are shown by the full line curves. Comparisons of Fig. 11 with Figs. 5 and 6 show values of U at a given value of K to be significantly higher for the negative values of Ma_{sr}. The elevation increases as Ma_{sr} becomes more negative and predominantly arises from the greater values of $K_{q\ell+}$ and $f_{-i}(s)$ at positive values of s. Furthermore, at the more negative values of Ma_{sr}, the high values of U persist to higher values of K, in contrast to the decline in U with K at positive values of Ma_{sr}. Another consequence of the high values of $K_{q\ell+}$ is that the effect of nonsteady flame stretch rates on flame extinction is reduced. With $K_{q\ell+} = 1.77$ (at $\phi = 1.5$) the condition $\eta \leqslant 1$ in Eq. (28) gives $K \leqslant 0.57$, as compared with values of about 0.1 for the positive values of Ma_{sr}.

At even more negative values of Ma_{sr} the flames become more unstable, with values of Pe_{cl}, as low as 200 or less [38]. The instability contribution to P_{bi} and U becomes appreciable, as shown for the former in Fig. 12. The values of the solid line curves are evaluated with Pe_{cl} obtained from Eq. (B.5), while the values of the broken line curves are for the lower value of $Pe_{cl} = 200$, but with the same values of Ma_{sr} as in Fig. 10. This low value of Pe_{cl} significantly increases the instability and P_{bi}, again particularly at high R_l and low K.

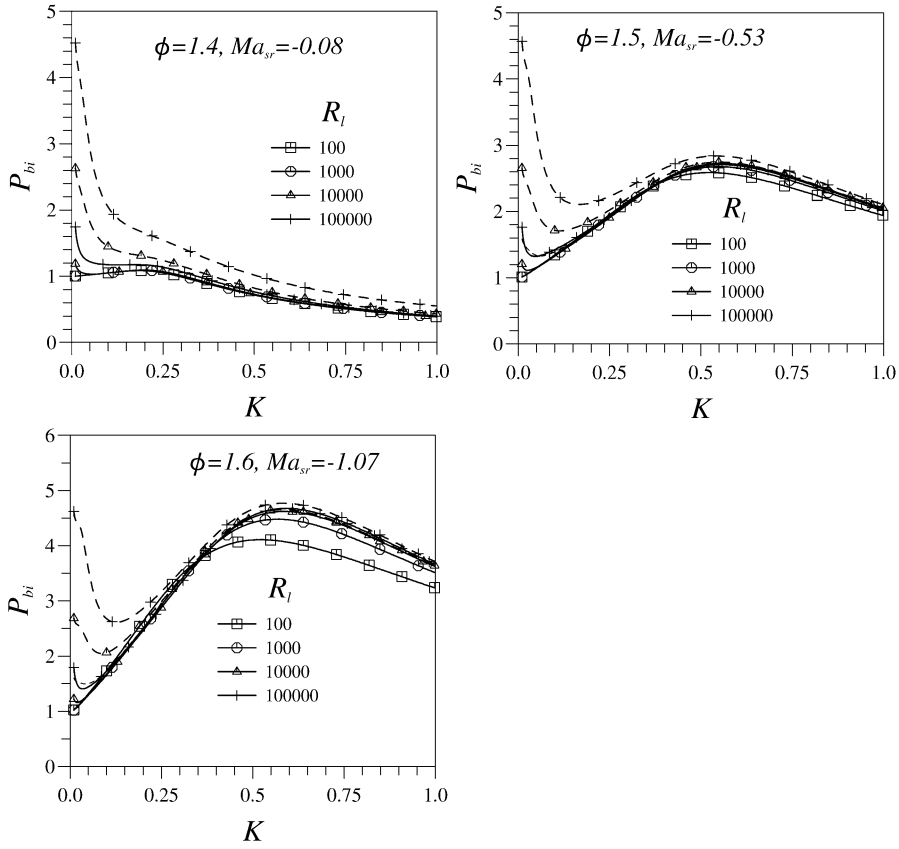

Fig. 12. $P_{\rm bi}$ versus K for three C_3H_8–air mixtures, with $\mathrm{Ma_{sr}} < 0$ and four values of R_l. Solid curves: $\mathrm{Pe_{cl}}$ from Eq. (B.5). Dashed curve: $\mathrm{Pe_{cl}} = 200$.

There are less experimental turbulent burning velocity data available for negative values of $\mathrm{Ma_{sr}}$ to check the predicted values of U. An increase in pressure decreases $\mathrm{Ma_{sr}}$ for CH_4–air mixtures and values eventually become negative [46]. Kobayashi and coworkers have measured u_t for such mixtures with $\phi = 0.9$, at different pressures on a high-pressure burner [6,7]. Values of u_t/u_ℓ were expressed as a function of both u'/u_ℓ and pressure ratio. Their data are expressed in Fig. 13 by the symbols, in terms of U versus K at the different pressures and values of $\mathrm{Ma_{sr}}$. Values of R_l were taken from [7]. Some of the experimental data are in the regime $u'_k/u_\ell \leqslant 1$, with small values of R_l, where the present analysis is inapplicable. In Fig. 13 this inapplicable regime corresponds approximately to $K \leqslant 0.05$.

The full line curves show computed values corresponding to the experimental conditions, with different values of u'/u_ℓ and R_l, and are terminated at the limit, $K = 0.05$. An exception is made at 0.1 MPa, $\mathrm{Ma_{sr}} = 3.52$, where they are extended beyond it. Values of $\mathrm{Ma_{sr}}$ up to a pressure of 1.0 MPa were obtained from [46], but thereafter had to be estimated. No data were known for $K_{q\ell+}$ at high pressures and these values also had to be estimated. However, the lower dotted curves in Fig. 10 suggest that values of $P_{\rm bi}$ and U are not too sensitive to $K_{q\ell+}$ at the more negative values of $\mathrm{Ma_{sr}}$.

Agreement between the computed and experimental points in Fig. 13 is satisfactory, although at pressures of 2 and 3 MPa the values of $\mathrm{Ma_{sr}}$ had to be estimated. As $\mathrm{Ma_{sr}}$ becomes more negative, so $\mathrm{Pe_{cl}}$ becomes small and it is increasingly difficult to assign an accurate value to it [38]. The experimental values of R_l do not exceed 2500 and the computations suggest that there are no elevations due to flamelet instabilities. Elevations on this count appear to be confined to the narrow regime of $K \leqslant 0.05$, $u'/u_\ell \leqslant 1$, in which the present analysis is inapplicable.

Cambray and Joulin [1,47] have analysed the effect of the Darrieus–Landau instability on flame front wrinkling in this regime and shown that as u'/u_ℓ approaches zero, there is a sharp increase in u_t with u'. For conditions close to those at 0.1 MPa and for the lowest experimental value of K in Fig. 13 with a positive value of $\mathrm{Ma_{sr}}$, their data suggest a value of U indicated by the triangle symbol on the figure. This is fairly close to the measured value. For the higher

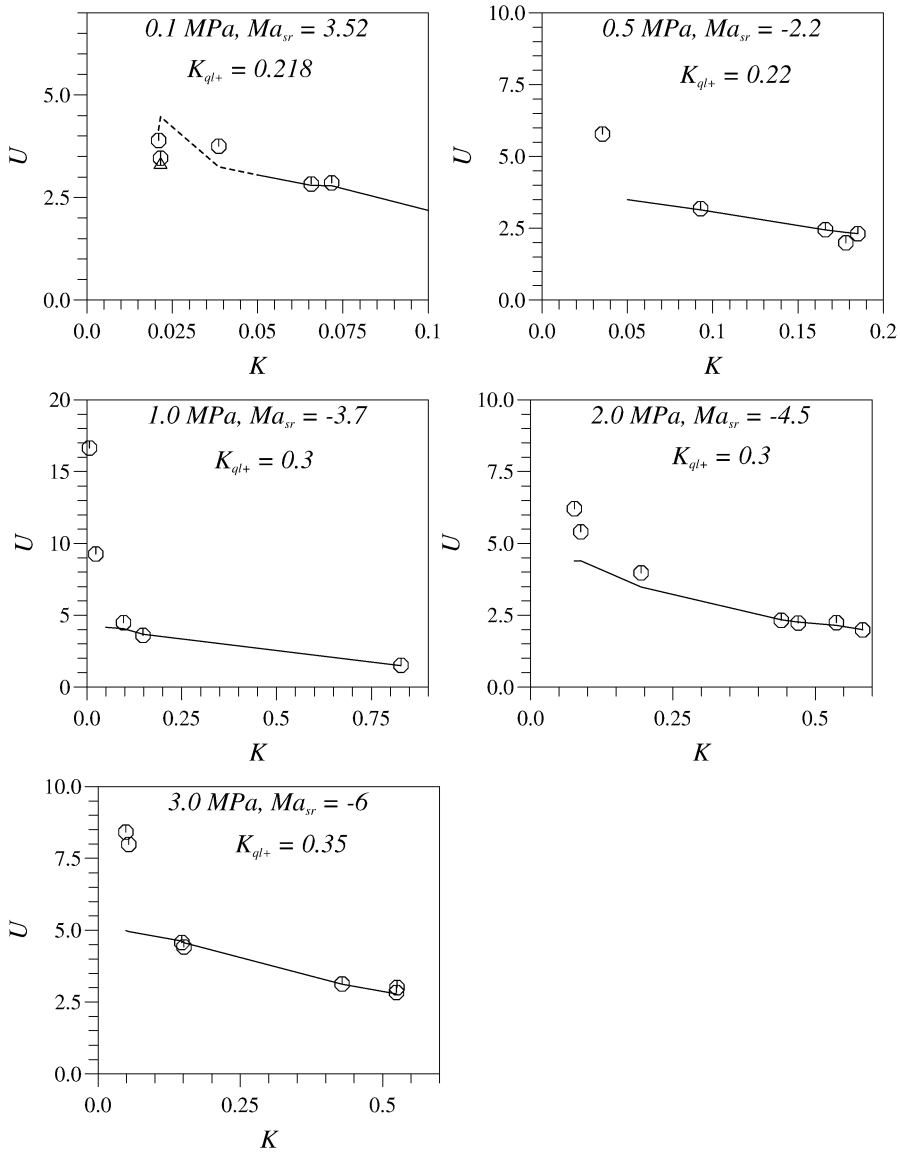

Fig. 13. Comparison of present computations of U for CH_4–air mixtures at five different pressures, $\phi = 0.9$ (solid curves) with experimental data (symbols) [6,7].

pressure points in this low K regime the experimental values of U are even higher. This is not surprising as the corresponding laminar flames exhibit burning velocity enhancements due to instabilities that can be appreciable for negative Markstein numbers [49].

9. Conclusions

The flame stretch factor in the expression for P_b has been modified to embrace flamelet wrinkling due to instabilities. The wavelengths of the wrinkling extend from an inner cutoff found from a combination of instability theory and experiment to an outer cutoff given by the integral length scale of the turbulence. Instabilities are generated below a critical value of the flame stretch rate, derived from experimental values of the critical Peclet number in laminar explosions.

A partial validation of the computed values of P_{bi} for positive values of Ma_{sr} has been provided by comparing values of U from Eq. (5) with experimental values. There is reasonable agreement between the two, but allowance for nonsteady effects appears to be necessary at the higher values of K. Enhancement of U due to instabilities is insignificant, except at high values of R_l and low values of K.

When $\mathrm{Ma_{sr}}$ is negative, both P_{bi} and U can become appreciably higher than when $\mathrm{Ma_{sr}}$ is positive, for otherwise comparable conditions. Again, results from the computational approach are in satisfactory agreement with experiment. The higher values of U persist to higher values of K with negative values of $\mathrm{Ma_{sr}}$ than with positive values. These strikingly high values arise from the combined effects of higher values of $K_{q\ell+}$ and of $f_{-i}(s)$ at positive values of s, as $\mathrm{Ma_{sr}}$ becomes more negative. Because of the apparently large effect of large values of $K_{q\ell+}$ there is an urgent need for experimental and computational data on flame stretch extinction at high pressures. It is also important to resolve whether large values of $K_{q\ell+}$ are linked to negative values of $\mathrm{Ma_{sr}}$. In addition to the effects of the very negative values of $\mathrm{Ma_{sr}}$, the correspondingly low values of $\mathrm{Pe_{cl}}$ enhance the onset of instabilities.

The mixed regime of $K \leqslant 0.05$, $u'/u_\ell \leqslant 1$ is outside the regime of the present modelling, but it is here that flame instability effects are appreciable, particularly at the more negative values of $\mathrm{Ma_{sr}}$, and these enhance the burning velocity. The burning velocities of the corresponding laminar flames are enhanced significantly by instabilities.

The most marked limitations in the present approach lie in the inadequate data at high temperatures and pressures for $\mathrm{Ma_{sr}}$, $K_{q\ell+}$, $\mathrm{Pe_{cl}}$, and u_ℓ for different fuel mixtures. There also is considerable uncertainty as to the influence of negative stretch rates on flame extinction. Much more work is needed, at all pressures, on negative stretch rate and $K_{q\ell+}$. Here, studies of inwardly propagating flames and burner flame tips are relevant. These might reveal the limitations of trying to combine the effects of both strain and flame curvature. The expressions for $f(s)$, Eq. (11), should be checked with other mixtures and at higher temperatures and pressures. For all these reasons, even within the limitations of the present analyses, it is difficult to predict U definitively at high pressures. Nevertheless, the paper suggests how the relevant factors influencing it might be quantified.

Acknowledgment

The support of EPSRC is gratefully acknowledged.

Appendix A

The flame stretch rate pdf of $p(s)$ based on the reaction surface expressed in the integral form in [30] can be manipulated into the algebraic form,

$$p(s) = -\frac{1}{2\sqrt{\pi}} a \frac{(2E\,\mathrm{Ma_{sr}}\,C_1 - d)}{d^2\sigma_s} e^{-G},$$

where

$$a = \frac{2.6R_l^{0.25}}{K^{0.5}},$$

$$d = \left(\frac{2}{15} + \frac{(aK\sigma_s)^2}{2} + 2(sK\,\mathrm{Ma_{sr}}\,C_1)^2 - \frac{4sK\,\mathrm{Ma_{sr}}\,C_1}{\sqrt{15}}\right)^{1/2} \Big/ K\sigma_s,$$

$$E = \sqrt{15}(\bar{a}_s - s)\left(1 - \sqrt{15}sK\,\mathrm{Ma_{sr}}\,C_1\right) \Big/ \left[15\sigma_s\left(\frac{2}{15} + \frac{(aK\sigma_s)^2}{2} + 2(sK\,\mathrm{Ma_{sr}}\,C_1)^2 - \frac{4sK\,\mathrm{Ma_{sr}}\,C_1}{\sqrt{15}}\right)^{1/2}\right],$$

$$G = \frac{15}{2}(aK)^2(\bar{a}_s - s)^2 \Big/ \left[15(aK\sigma_s)^2 + 60(sK\,\mathrm{Ma_{sr}}\,C_1)^2 - 8\sqrt{15}sK\,\mathrm{Ma_{sr}}\,C_1 + 4\right].$$

The normalised rms strain rate is σ_s and s is the normalised flame stretch rate. The values of C_1 are given with Eq. (B.2a) and depend upon the sign of $\mathrm{Ma_{sr}}$.

Appendix B

B.1. Value of s_{cl}

The critical stretch rate, s_{cl}, below which flamelets become unstable and wrinkle is found from the critical dimensionless spherical flame radius at which cells appear and the flame speed increases. This is the critical Peclet number, $\mathrm{Pe_{cl}}$, defined by this flame radius, r, normalised by δ_ℓ. At higher Peclet numbers where the stretch rates are below the critical value, the flame is unstable and it is shown in [30] that

$$s_{\mathrm{cl}} = \left(\frac{2}{\mathrm{Pe_{cl}}}\frac{\mathrm{d}r}{\mathrm{d}t}\right) \Big/ \left(u_\ell K\sqrt{15}\right). \tag{B.1}$$

In [22], the flame speed, $\mathrm{d}r/\mathrm{d}t$, is given by $(u_{\mathrm{n}}/S) \times (\rho_{\mathrm{u}}/\rho_{\mathrm{b}})$, where S is a flame speed factor, of order unity, values of which are given as a function of Pe and $(\rho_{\mathrm{u}}/\rho_{\mathrm{b}})$. This can be reexpressed in terms of u_{nr}. The necessary expressions for u_{nr}/u_ℓ and u_{n}/u_ℓ are given in [30] by

$$u_{\mathrm{nr}}/u_\ell \approx 1 - s\,\mathrm{Ma_{sr}}\,C_1 K\sqrt{15}, \quad \begin{cases} C_1 = 0.925, & \mathrm{Ma_{sr}} \geqslant 0, \\ C_1 = 1.480, & \mathrm{Ma_{sr}} < 0, \end{cases} \tag{B.2a}$$

and

$$u_n/u_\ell \approx 1 - s(\rho_u/\rho_b - 1)\,\mathrm{Ma_{sr}}\,C_2 K\sqrt{15},$$
$$\begin{cases} C_2 = -0.125, & \mathrm{Ma_{sr}} \geqslant 0, \\ C_2 = 1.225, & \mathrm{Ma_{sr}} < 0. \end{cases} \quad \text{(B.2b)}$$

These values of C_1 and C_2 are those appropriate to a flame surface located at the start of the reaction zone. From Eq. (20) in [22] and Eqs. (B.1) and (B.2a),

$$s_{cl} = \frac{2C_s}{\mathrm{Pe_{cl}}\,K\,S\sqrt{15}}\left(\frac{\rho_u}{\rho_b}\right) \times \left(1 + \left(\frac{\rho_u}{\rho_b}\right)\frac{2C_sC_1\,\mathrm{Ma_{sr}}}{S\,\mathrm{Pe_{cl}}}\right)^{-1}, \quad \text{(B.3)}$$

in which

$$C_s = (1 - \rho_u/\rho_b)(1 - \rho_u/S\rho_b)^{-1}. \quad \text{(B.4)}$$

Although theoretical values of $\mathrm{Pe_{cl}}$ can be obtained for spherical flames from the linear instability theory of Bechtold and Matalon [48], these values are less than those at which full cellularity appears in experiments. Consequently, experimental values of $\mathrm{Pe_{cl}}$ were employed and these have been correlated in terms of $\mathrm{Ma_{sr}}$ by [46]

$$\mathrm{Pe_{cl}} = 177\,\mathrm{Ma_{sr}} + 2177, \quad \text{(B.5)}$$

although this relationship is less reliable at increasingly negative values of $\mathrm{Ma_{sr}}$.

B.2. Values of l_s/δ_ℓ

The apparent time lag in the development of full cellularity in the theory of Bechtold and Matalon results in an overestimation of the larger theoretical unstable wavenumber, n_s. In [33] this was reduced by multiplying the theoretical values of n_s by a constant less than unity, f. The value of this was such that $(fn_s)_{cl}$ was equal to the smaller wavenumber at the measured $\mathrm{Pe_{cl}}$, namely $(n_l)_{cl}$. This is located at the tip of a peninsula of unstable wavenumbers which is bounded by a value of n_l that is almost constant and one of fn_s that increases linearly with Pe.

The adaptation in [33] of the instability theory of Bechtold and Matalon [48] shows that in unstable flames l_s/δ_ℓ soon attains a constant value that depends upon $\mathrm{Ma_{sr}}$ and ρ_u/ρ_b, and is given by

$$l_s/\delta_\ell = 2\pi/(\mathrm{d}fn_s/\mathrm{d\,Pe}). \quad \text{(B.6)}$$

This expression enabled the inner cutoff l_s/δ_ℓ to be evaluated in the valid regime of $\mathrm{Ma_{sr}} > 3.0$. The smallest values of l_s/δ_ℓ at a given value of Pe occur at the smallest values of $\mathrm{Ma_{sr}}$.

The procedures for evaluating l_s/δ_ℓ are described more fully in [49]. For $\mathrm{Ma_{sr}} < 3$ recourse to experiment was necessary. In the cascade of decreasing wavelengths observed in [38] the smallest cells appeared to be in dynamic equilibrium. They increased in size as the flame kernel grew. This decreased the localised flame stretch rate and, consequently, such cells became unstable. They restabilised by fissioning into smaller cells, with higher, stabilising, local stretch rates. Just prior to fissioning, the normalised wavelength of a localised cell, l_s/δ_ℓ, was observed to be close to that of the original flame kernel at the critical Peclet number, $\mathrm{Pe_{cl}}$, just prior to the development of cellularity. Hence,

$$l_s/\delta_\ell = 2\pi\,\mathrm{Pe_{cl}}/(n_l)_{cl}, \quad \text{(B.7)}$$

where $(n_l)_{cl}$ is the wavenumber at $\mathrm{Pe_{cl}}$, which could be found with sufficient accuracy from [48]. This expression was used for $\mathrm{Ma_{sr}} \leqslant 3$.

However, for the most unstable flames when $\mathrm{Ma_{sr}}$ was highly negative (say < -4), there appeared to be a lower physicochemical limit to the value of the wavelength of a localised cell, l_s/δ_ℓ, below which a wrinkled flame sheet could not be maintained. It might be surmised that this occurs at the order of the flame thickness and the diagnostic studies in [38] suggested that, in this case, the inner cutoff was at $l_s/\delta_\ell \approx 50$.

In the unstable regime $s_{cl} \geqslant s \geqslant s_{q-}$, in Eqs. (13a) and (13b), we write

$$u_{nri}/u_\ell = (u_{nri}/u_{nr})(u_{nr}/u_\ell) \quad \text{for positive values of } \mathrm{Ma_{sr}}, \quad \text{(B.8a)}$$

$$u_{ni}/u_\ell = (u_{ni}/u_n)(u_n/u_\ell) \quad \text{for negative values of } \mathrm{Ma_{sr}}. \quad \text{(B.8b)}$$

Equations (14a), (B.8a), and (13a), after some manipulation, yield

$$f_{+i}(s) = f_+(s) + 0.8\left[(l/l_s)^{1/3} - 1\right](u_{nr}/u_\ell) \quad \text{for } s_{cl} \geqslant s \geqslant s_{q-}. \quad \text{(B.9)}$$

For the remaining part of the spectrum, $s_{q+} \geqslant s \geqslant s_{cl}$, where the flamelets are stable, $f_+(s)$ is unchanged. With Eq. (B.2a), Eq. (B.9) becomes

$$f_{+i}(s) = f_+(s) + 0.8\left[(l/l_s)^{1/3} - 1\right] \times \left[1 - s\,\mathrm{Ma_{sr}}\,C_1 K\sqrt{15}\right]. \quad \text{(B.10a)}$$

By similar reasoning for negative values of $\mathrm{Ma_{sr}}$ and invoking Eq. (B.2b),

$$f_{-i}(s) = f_-(s) + 0.8\left[(l/l_s)^{1/3} - 1\right] \times \left[1 - s(\rho_u/\rho_b - 1)\,\mathrm{Ma_{sr}}\,C_2 K\sqrt{15}\right]. \quad \text{(B.10b)}$$

Again, for the remaining part of the spectrum, $s_{q+} \geqslant s \geqslant s_{cl}$, $f_-(s)$ is unchanged.

References

[1] P. Cambray, G. Joulin, Combust. Sci. Technol. 97 (1994) 405–428.
[2] R.N. Paul, K.N.C. Bray, Proc. Combust. Inst. 26 (1996) 259–266.
[3] H. Boughanem, A. Trouvé, Proc. Combust. Inst. 27 (1998) 971–978.
[4] V. Bychkov, Phys. Rev. E 68 (2003) 066304.
[5] H. Kobayashi, H. Kawazoe, Proc. Combust. Inst. 28 (2000) 375–382.
[6] H. Kobayashi, T. Tamura, K. Maruta, T. Niioka, F. Williams, Proc. Combust. Inst. 26 (1996) 389–396.
[7] H. Kobayashi, Y. Kawabata, K. Maruta, Proc. Combust. Inst. 27 (1998) 941–948.
[8] C.K. Law, D.L. Zhu, G. Yu, Proc. Combust. Inst. 21 (1986) 1419–1426.
[9] P.A. Libby, F.A. Williams (Eds.), Turbulent Reacting Flows, Academic Press, London, 1994.
[10] N. Peters, Turbulent Combustion, Cambridge Univ. Press, Cambridge, UK, 2000.
[11] D.B. Spalding, Proc. Combust. Inst. 13 (1971) 649–657.
[12] D. Bradley, P.H. Gaskell, X.J. Gu, M. Lawes, M.J. Scott, Combust. Flame 115 (1998) 515–538.
[13] D. Bradley, D.R. Emerson, P.H. Gaskell, X.J. Gu, Proc. Combust. Inst. 29 (2002) 2155–2162.
[14] A.Y. Klimenko, R.W. Bilger, Prog. Energy Combust. Sci. 25 (1999) 595–687.
[15] S.B. Pope, Prog. Energy Combust. Sci. 11 (1985) 119–192.
[16] F. di Mare, W.P. Jones, K.R. Menzies, Combust. Flame 137 (2004) 278–294.
[17] K.N.C. Bray, M. Champion, P. Libby, Combust. Flame 127 (2001) 2023–2040.
[18] D. Veynante, L. Vervisch, Prog. Energy Combust. Sci. 28 (2002) 193–266.
[19] T. Poinsot, D. Veynante, S. Candel, J. Fluid Mech. 228 (1991) 561.
[20] T. Poinsot, S. Candel, A. Trouvé, Prog. Energy Combust. Sci. 21 (1996) 531–576.
[21] D. Bradley, P.H. Gaskell, X.J. Gu, Proc. Combust. Inst. 27 (1998) 849–856.
[22] D. Bradley, P.H. Gaskell, X.J. Gu, Combust. Flame 104 (1996) 176–198.
[23] S. Candel, T. Poinsot, Combust. Sci. Technol. 70 (1990) 1–15.
[24] K.N.C. Bray, Proc. R. Soc. London A 431 (1990) 315–335.
[25] D. Bradley, P.H. Gaskell, X.J. Gu, Combust. Flame 96 (1994) 221–248.
[26] D. Bradley, Proc. Combust. Inst. 24 (1992) 247–262.
[27] D. Bradley, Combust. Theory Model. 6 (2002) 361–382.
[28] R.G. Abdel-Gayed, D. Bradley, M. Lawes, Proc. R. Soc. London A 414 (1987) 389–413.
[29] P.K. Yeung, S.S. Girimaji, S.B. Pope, Combust. Flame 79 (1990) 340–365.
[30] D. Bradley, P.H. Gaskell, X.J. Gu, A. Sedaghat, Combust. Flame 135 (2003) 503–523.
[31] J.H. Chen, H.G. Im, Proc. Combust. Inst. 27 (1998) 819–826.
[32] J.O. Sinibaldi, J.F. Driscoll, C.J. Mueller, J.M. Donbar, C.D. Carter, Combust. Flame 133 (2003) 323–334.
[33] D. Bradley, Philos. Trans. R. Soc. London A 357 (1999) 3567–3581.
[34] Yu.A. Gostintsev, A.G. Istratov, V.E. Fortov, Akad. Nauk 353 (1997) 55–56.
[35] Yu.A. Gostintsev, A.G. Istratov, Yu.V. Shulenin, Combust. Explosion Shock Waves (March 1989) 563–569.
[36] D. Bradley, Combust. Sci. Technol. 158 (2000) 15–33.
[37] D. Bradley, T.M. Cresswell, J.S. Puttock, Combust. Flame 124 (2001) 551–559.
[38] D. Bradley, C.G.W. Sheppard, R. Woolley, D.A. Greenhalgh, R.D. Lockett, Combust. Flame 122 (2000) 195–209.
[39] D. Bradley, A.K.C. Lau, M. Lawes, Philos. Trans. R. Soc. London A 338 (1992) 359–387.
[40] T. Echekki, M.G. Mungal, Proc. Combust. Inst. 23 (1990) 455–461.
[41] A.F. Ibarreta, J.F. Driscoll, D.A. Feikema, Proc. Combust. Inst. 29 (2002) 1435–1443.
[42] R.G. Abdel-Gayed, D. Bradley, Combust. Flame 62 (1985) 61–68.
[43] C. Meneveau, T. Poinsot, Combust. Flame 86 (1991) 311–332.
[44] F.N. Egolfopoulos, C.S. Campbell, J. Fluid Mech. 318 (1996) 1–29.
[45] J.M. Donbar, J.F. Driscoll, C.D. Carter, Combust. Flame 125 (2001) 1239–1257.
[46] X.J. Gu, M.Z. Haq, M. Lawes, R. Woolley, Combust. Flame 121 (2000) 41–58.
[47] P. Cambray, G. Joulin, Proc. Combust. Inst. 24 (1992) 61–67.
[48] J.K. Bechtold, M. Matalon, Combust. Flame 67 (1987) 77–90.
[49] A.S. Al-Shahrany, D. Bradley, M. Lawes, R. Woolley, Proc. Combust. Inst. 30 (2005) 225–232.